UV-Induced Photoisomerization of Acetylacetone and Identification of Less-Stable Isomers by Low-Temperature Matrix-Isolation Infrared Spectroscopy and Density Functional Theory Calculation

Naoko Nagashima, Satoshi Kudoh, Masao Takayanagi, and Munetaka Nakata*

Graduate School of BASE (Bio-Applications and Systems Engineering), Tokyo University of Agriculture and Technology, 2-24-16 Naka-cho, Koganei, Tokyo 184-8588, Japan

Received: July 5, 2001; In Final Form: September 21, 2001

UV-induced photoisomerization of acetylacetone in low-temperature argon matrixes has been studied by Fourier transform infrared spectroscopy. Identifications of the species produced by UV irradiation ($\lambda > 280$ nm) were carried out with the aid of the density functional theory (DFT) calculation, in which the 6-31G* basis set was used to optimize the geometrical structures. By comparison of the observed infrared bands with the calculated spectral patterns, it was found that cis−trans isomerization around the C−C, C═C, and C−O bonds occurs to produce less-stable enol isomers, 2-hydroxy-2-penten-4-one. Shorter-wavelength irradiation ($\lambda < 280$ nm) induced hydrogen-atom migration of the enol isomers to produce a keto isomer, 2,4-pentanedione.

Introduction

Acetylacetone has been studied by a number of physical and organic chemists with particular attention to (1) keto−enol tautomerization (see Scheme 1), (2) equilibrium symmetry of enol isomer, C_s or C_{2v} (see Scheme 2), and (3) its photoisomerization. For example, keto−enol tautomerization has been studied by photoelectron spectroscopy,[1] NMR,[2,3] infrared spectroscopy,[4−6] and ab initio calculations.[7,8]

It was concluded that the enol isomer, which has an intramolecular hydrogen bonding and a conjugated π-electron system, mainly exists in the gas phase[9] and in solution,[2] while tautomeric equilibrium shifts toward the keto isomer in solution as the solvent polarity is increased.[2,10]

The structure of enol isomer has also been studied experimentally[10−12] and theoretically.[13−18] For example, Cohen and Weiss[11] measured infrared spectra of acetylacetone in solution at various temperatures and assumed that C_s and C_{2v} isomers exist in solution. The double-minimum potential on hydrogen-atom transfer has stirred up the interest of theorists in hydrogen tunneling. Dannenberg and Rios[14] reported by an MP2/D95++** calculation that C_{2v} was more stable than C_s by 0.2 kcal mol^{-1}, but Buemi and Gandolfo[16] performed an AM1 calculation, resulting in the conclusion that C_s was the most stable structure. Marvi and Grdadolnik[17,18] examined the proton potential at various ab initio and density functional theory (DFT) levels and pointed out that C_{2v} is not at the minimum but on the barrier, where the proton donor−acceptor distance influences the barrier height.

In contrast to subjects 1 and 2, fewer papers on photoisomerization of the enol isomer have been published. As shown in Figure 1, the enol isomer has three rotational axes; trans (T) and cis (C) conformations around each axis allow eight isomers, CCC, CCT, etc., where the symbols apply to the C2−C3, C3═C4, and C4−O5 bonds in this order. Vereiov et al. studied UV-induced isomerization of acetylacetone in liquid and found that the hydrogen bonding of CCC was broken.[19] Roubin and co-workers[20,21] studied UV-induced isomerization in xenon matrixes and observed infrared bands of at least three new species, which were assumed to be CCT, TCC, and TCT. However, their assignment, which was not based on detailed spectral analyses, is doubtful.

SCHEME 1

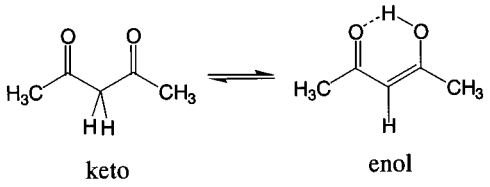

SCHEME 2

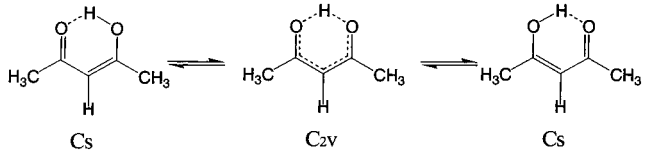

Recent quantum chemical calculations can provide accurate vibrational wavenumbers for small molecules. Especially, most of the vibrational wavenumbers predicted by DFT calculations[22,23] are shown to be consistent with the corresponding observed bands within 10 cm^{-1} if a suitable scaling factor is used.[24−32] Thus predictions by DFT calculations have enabled correct identification of conformers among various possibilities no matter whether their spectral patterns are overlapped with one another.

In the present work, UV-induced isomerization of acetylacetone in argon matrixes has been studied. Infrared bands of less-stable isomers are measured and identified by a comparison with the spectral patterns predicted by DFT calculations.

Experimental Section

A sample of acetylacetone (more than 99.0% purity), purchased from Wako Pure Chemicals Industry, was used after

* To whom correspondence should be addressed. E-mail: necom@cc.tuat.ac.jp. Tel: +81-42-388-7349. Fax: +81-42-388-7349.

10.1021/jp012557m CCC: $20.00
Published on Web 11/08/2001

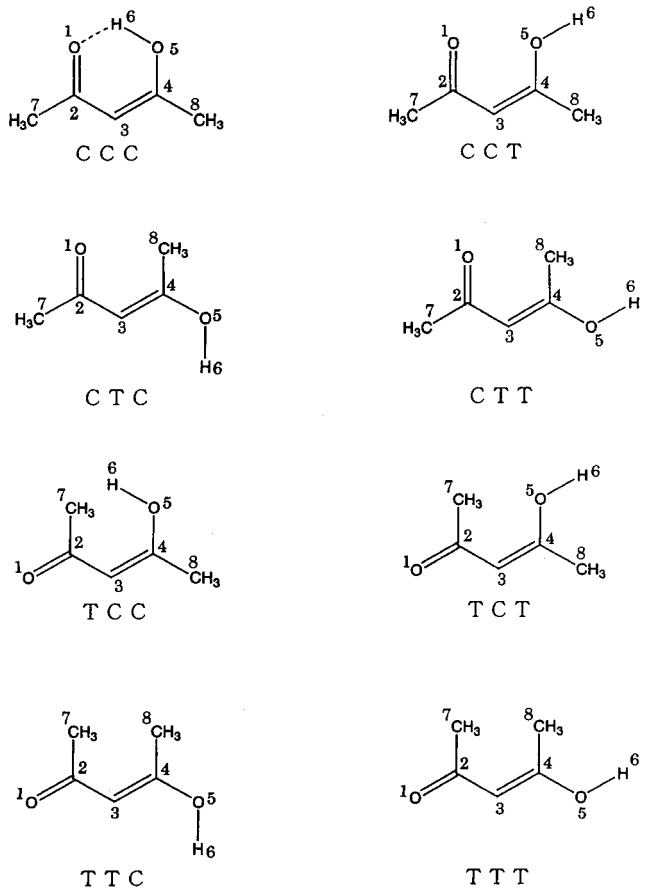

Figure 1. Eight possible isomers of enol-type acetylacetone and numbering of atoms.

removing water with magnesium sulfate. The sample vapor was premixed with argon gas (Nippon Sanso, more than 99.9999% purity) in a glass bulb. The mixing ratio of acetylacetone/argon was about 1/2000. The premixed gas was deposited on a CsI plate at 15 K cooled by a closed-cycle helium refrigeration unit. A superhigh-pressure mercury lamp was used to induce photoisomerization. The UV light was introduced on the matrix sample through a water filter of 50 mm diameter and 100 mm length and a quartz lens of 50 mm diameter and 200 mm focal length. An optical short-cut filter, UV-28, was used to remove shorter-wavelength radiation (λ < 280 nm). Infrared spectra were measured with an FTIR spectrophotometer (JEOL, model JIR-7000). The spectral resolution was 0.5 cm^{-1}, and the number of accumulations was 64. Other experimental details are reported elsewhere.[25]

Results and Discussion

DFT Calculations. *(1) Optimized Geometry and Relative Energy.* DFT calculations were performed by using the Gaussian 98 program[33] with the 6-31G* basis set, in which the hybrid density functional,[34] in combination with the Lee−Yang−Parr correlation functional (B3LYP),[35] was used to optimize the geometrical structures. Our calculation reconfirmed the conclusion of Marvi and Grdadolnik[17,18] that the optimized geometry of CCC has C_s symmetry. The C_{2v} structure is less stable than the C_s structure by 12 kJ mol^{-1} and on the maximum of the potential; the wavenumber of one vibrational mode is imaginary.

The calculated bond distances and angles of the skeletons for eight enol isomers and their relative energies are summarized in Table 1. All of the atoms are placed on a plane except for a part of the hydrogen atoms of the methyl groups, for which all

TABLE 1: Optimized Geometry (bond lengths, *r*, in Å and bond angles, ∠, in deg)[a] and Relative Energy (kJ mol^{-1}) for Eight Enol Isomers

isomer	CCC	CCT	CTC	CTT	TCC	TCT	TTC	TTT
ΔE^b	0.0	71.9	48.8	53.5	59.5	64.4	67.1	78.9
r(O1═C2)	1.250	1.224	1.228	1.230	1.226	1.227	1.227	1.227
r(C2−C3)	1.445	1.473	1.471	1.469	1.469	1.476	1.473	1.472
r(C3═C4)	1.372	1.354	1.358	1.354	1.357	1.350	1.355	1.352
r(C4−O5)	1.328	1.354	1.358	1.362	1.357	1.365	1.363	1.368
r(O5−H6)	1.009	0.970	0.972	0.970	0.970	0.969	0.972	0.969
r(C2−C7)	1.515	1.527	1.525	1.524	1.530	1.519	1.523	1.525
r(C4−C8)	1.498	1.504	1.494	1.498	1.500	1.503	1.499	1.502
∠(O1═C2−C3)	121.9	124.0	125.0	125.1	120.0	118.8	118.2	118.3
∠(C2−C3═C4)	120.6	126.2	126.7	126.3	130.6	129.6	132.6	132.3
∠(C3═C4−O5)	122.3	121.4	121.6	117.1	126.9	121.4	120.6	115.9
∠(C4−O5−H6)	105.7	109.2	109.3	109.2	110.7	109.3	109.2	109.7
∠(O1═C2−C7)	119.5	120.8	120.1	120.0	119.1	120.5	119.1	118.8
∠(O5−C4−C8)	113.6	115.7	111.0	115.9	110.1	115.3	108.8	113.8

[a] Other structural parameters are available upon request. [b] Relative energies.

of the isomers have C_s symmetry. It is found that CCC is the most stable isomer, which has intramolecular hydrogen bonding between the O−H and C═O groups and a π-conjugated system. The O−H distance for CCC, 1.009 Å, is longer than that for other isomers, 0.969−0.972 Å. The O═C and C═C bonds for CCC, 1.250 and 1.372 Å, are longer than those for other isomers, 1.224−1.230 and 1.350−1.358 Å, for the same reason. The second stable isomer is CTC, which is formed from CCC by isomerization around the C═C bond. TTC and TTT are less stable because they have repulsion between two methyl groups, while CCT has repulsion between two oxygen atoms, as shown in Figure 1. The order of relative energies is

$$\text{CCC} < \text{CTC} < \text{CTT} < \text{TCC} < \text{TCT} < \text{TTC} < \text{CCT} < \text{TTT}$$

Chiavassa et al.[36,37] performed ab initio calculations for eight enol isomers of malonaldehyde at the DZP/MP2 level and obtained optimized geometries and relative energy. The order of the energies is

$$\text{CCC} < \text{TTC} < \text{CTC} < \text{CTT} < \text{TTT} < \text{TCT} \approx \text{TCC} < \text{CCT}$$

Their order for malonaldehyde seems to be consistent with ours for acetylacetone excluding TTC and TTT. Because malonaldehyde has no repulsion between the methyl groups, TTC and TTT are relatively stabilized in comparison with the corresponding isomers of acetylacetone.

We also performed a DFT calculation for the keto isomer. The relative energy of this isomer is higher than that of CCC by 13.5 kJ mol^{-1} but is at least 35 kJ mol^{-1} lower than that of the other enol isomers, which have no intramolecular hydrogen bonding. The optimized geometry of the keto isomer shows a nonplanar skeleton and has C_2 symmetry; the dihedral angle between the two C═O groups is 88.2°. The C═O, C−C, and C−CH_3 bond distances are calculated to be 1.215, 1.538, and 1.513 Å, respectively, while the bond angles of O═C−C, C−C−C, O═C−CH_3, and CH_3−C−C are 120.7°, 107.6°, 122.3°, and 115.9°, respectively.

(2) Vibrational Wavenumbers and Relative Intensities. We also calculated vibrational wavenumbers and relative intensities of the isomers, as summarized in Table 2. The O−H stretching mode for CCC is expected to appear around 3000 cm^{-1}, which is lower than the other isomers by 700 cm^{-1}. This large shift is due to intramolecular hydrogen bonding. The most intense bands for all of the isomers are due to C═O and C═C stretching

TABLE 2: Calculated Vibrational Wavenumbers (cm^{-1})[a] and Relative Intensities[b] of Eight Enol Isomers

CCC	CCT	CTC	CTT	TCC	TCT	TTC	TTT
3226 (2)	3738 (15)	3714 (5)	3745 (17)	3760 (19)	3757 (32)	3721 (9)	3753 (28)
3168 (4)	3199 (3)	3204 (1)	3192 (2)	3217 (1)	3216 (2)	3226 (1)	3222 (1)
3160 (4)	3164 (4)	3168 (2)	3188 (2)	3167 (3)	3165 (6)	3164 (3)	3198 (1)
3115 (3)	3158 (2)	3138 (4)	3167 (4)	3159 (2)	3162 (3)	3143 (5)	3163 (6)
3110 (3)	3100 (5)	3107 (2)	3104 (4)	3110 (3)	3123 (5)	3116 (3)	3113 (6)
3059 (6)	3081 (5)	3103 (3)	3077 (5)	3082 (4)	3079 (8)	3112 (2)	3080 (6)
3053 (2)	3043 (2)	3055 (4)	3047 (1)	3057 (4)	3062 (1)	3064 (4)	3051 (3)
3026 (91)[c]	3033 (7)	3046 (1)	3028 (9)	3021 (3)	3031 (12)	3053 (2)	3035 (11)
1706 (100)	1789 (36)	1771 (24)	1771 (43)	1754 (65)	1753 (90)	1744 (52)	1744 (85)
1676 (92)	1706 (100)	1671 (100)	1697 (100)	1697 (100)	1738 (100)	1701 (100)	1729 (100)
1518 (15)	1518 (2)	1525 (2)	1536 (3)	1526 (3)	1516 (0)	1522 (0)	1528 (0)
1504 (2)	1509 (2)	1506 (1)	1505 (2)	1517 (1)	1508 (5)	1516 (9)	1521 (4)
1499 (3)	1506 (3)	1499 (2)	1498 (1)	1512 (7)	1503 (3)	1501 (4)	1507 (7)
1498 (3)	1498 (3)	1491 (13)	1494 (4)	1500 (3)	1488 (9)	1498 (1)	1500 (2)
1485 (48)	1450 (10)	1481 (3)	1452 (67)	1452 (14)	1443 (13)	1467 (4)	1446 (21)
1438 (10)	1437 (2)	1419 (6)	1419 (16)	1418 (8)	1418 (21)	1423 (1)	1410 (41)
1418 (26)	1405 (12)	1407 (3)	1406 (4)	1404 (24)	1400 (37)	1412 (9)	1408 (56)
1410 (11)	1327 (82)	1331 (4)	1327 (5)	1336 (17)	1318 (81)	1308 (15)	1312 (18)
1286 (46)	1215 (23)	1244 (11)	1251 (38)	1291 (40)	1291 (66)	1278 (47)	1264 (40)
1205 (5)	1201 (3)	1199 (37)	1191 (37)	1159 (24)	1178 (5)	1234 (61)	1229 (90)
1078 (1)	1080 (1)	1090 (0)	1089 (0)	1081 (1)	1080 (1)	1081 (0)	1078 (0)
1054 (3)	1048 (3)	1050 (1)	1051 (2)	1050 (3)	1057 (5)	1053 (2)	1052 (3)
1045 (3)	1047 (0)	1045 (9)	1044 (3)	1045 (8)	1045 (0)	1035 (3)	1036 (1)
1017 (4)	999 (6)	997 (2)	991 (2)	1001 (8)	1017 (16)	1029 (8)	1026 (1)
960 (30)	921 (0)	957 (11)	956 (25)	945 (6)	933 (23)	917 (5)	904 (21)
951 (1)	891 (18)	852 (1)	875 (5)	860 (4)	864 (10)	868 (11)	901 (9)
926 (10)	823 (5)	835 (7)	848 (2)	802 (1)	814 (4)	794 (0)	788 (0)
790 (10)	650 (0)	632 (7)	634 (11)	622 (3)	623 (0)	588 (2)	584 (3)

[a] Nonscaling. [b] Relative intensities are in parentheses. [c] O−H stretching.

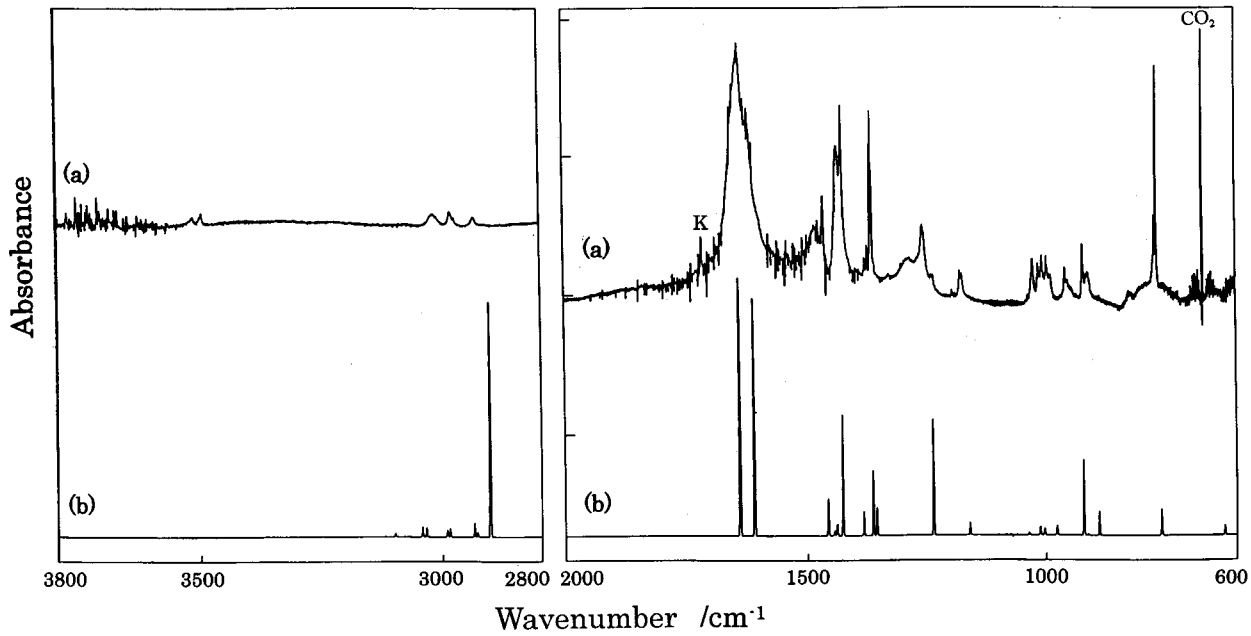

Figure 2. Infrared spectrum measured after sample deposition and before UV irradiation and calculated spectral pattern of CCC: (a) observed in an argon matrix; (b) calculated by the DFT/B3LYP/6-31G*. Most bands are assigned to CCC enol isomer. A band marked with "K" is assigned to keto isomer.

modes appearing around 1700 cm^{-1}, where these bands are more or less mixed with each other. Their relative intensities depend on the differences in the wavenumbers; they become closer as the difference decreases. For example, the difference between the C═O and C═C stretching bands for TCT is 15 cm^{-1}, and the intensity of the 1753 cm^{-1} band is nearly equal to that of the 1738 cm^{-1} band. On the other hand, the difference between the C═O and C═C stretching bands for CTC is 100 cm^{-1}, and the intensity of the 1771 cm^{-1} band is about 24% of that of the 1671 cm^{-1} band. These findings are useful for identification of isomers, as described later.

Identification of Infrared Bands. *(1) CCC Isomer.* The infrared spectrum of acetylacetone in an argon matrix was recorded after sample deposition and before UV irradiation. The observed spectrum shown in Figure 2a is essentially equal to that reported previously.[12,21] Some bands, especially in C═O and C═C stretching regions, are broad even in low-temperature rare-gas matrixes, probably because of intramolecular hydrogen

TABLE 3: Observed and Calculated Wavenumbers (cm^{-1}) for CCC Isomer

present work			reference[a]		
		observed	observed		
mode[b]	calcd[c]	Ar matrix	Ar matrix	Xe matrix	calcd[d]
C−H str	3097				
C−H str (Me)	3041				
C−H str (Me)	3034	3015	3012	3009	
C−H str (Me)	2990	2979	2974	2963	3148
C−H str (Me)	2986	2972			
C−H str (Me)	2937	2933			
C−H str (Me)	2931	2916			
O−H str	2905	*e*	*e*	*e*	2626
C═O str/ring str	1638	1636	1635	1634	1641
C═C str/ring str	1609	1616	1616	1610	1595
CH def (Me)	1457	1462	1459	1445	1445
CH def (Me)	1444				
CH def (Me)	1439				
CH def (Me)	1438				
ring def	1426	1432	1432	1426	
CH def (Me)	1380	1374			
ring def	1361	1360	1360		
CH def (Me)	1354	1280	1283	1288	1334
ring def	1235	1251	1251	1247	1260
CH def	1157	1174	1172	1170	1131
CH def (Me)	1035	1024			
CH def (Me)	1012	1013	1018	1016	
CH def (Me)	1003	996	1005	995	958
CH def (Me)	976	958	958	943	1001
O−H op	922	921	921	909	892
ring def	913	911			
ring def	889				
C−H op	758	769	764	774	783

[a] Reference 21. [b] Typical mode is denoted. [c] DFT/B3LYP/6-31G* level. A scaling factor of 0.96 is used. [d] Transferred LSD force field. [e] O−H stretching band has not been observed.

bonding. The O−H stretching band is too broad to be detected, probably for the same reason. This fact is supported by previous studies.[12,21] The weak peaks observed at 3500 cm^{-1} seem to be due to a negligible amount of water interacting with acetylacetone.

The calculated spectral pattern of the CCC isomer, shown in Figure 2b, in which a scaling factor of 0.96 is used is compared with the observed spectrum. This factor is recommended by Wong[38] and Scott and Radom,[39] who independently compared the observed wavenumbers for 1066 vibrational modes for 122 molecules with the corresponding values calculated by the DFT/B3LYP/6-31G* method. The calculated pattern of the CCC isomer is found to be in approximate agreement with the observed spectrum, although the relative intensities of some bands are slightly inconsistent.

The observed and calculated wavenumbers are summarized in Table 3 with their relative intensities. The C═O and C═C stretching bands are not clearly distinguishable; the weaker 1616 cm^{-1} band is observed at the shoulder of the stronger 1636 cm^{-1} band. The difference, 20 cm^{-1}, is roughly consistent with the calculated value, 30 cm^{-1}. A weak peak appearing at 1711 cm^{-1}, marked with K, is probably due to the keto isomer, as described later. It is concluded that the CCC isomer with C_s symmetry is a major species in the matrix sample before UV irradiation.

(2) CTC Isomer. When the matrix sample was exposed to the UV light from a superhigh-pressure mercury lamp through UV-28 cut and water filters, photoisomerization was induced. The temperature of the matrix sample was monitored by a thermocouple and confirmed to be unchanged before and during UV irradiation. The difference spectrum between those spectra measured before and after 2-min UV irradiation is shown in Figure 3a. Decreasing and increasing bands are due to a reactant CCC and photoproducts, respectively. The increasing bands marked with a circle (○) are assigned to a single species judging from the absorbance-growth behavior. The O−H stretching band of the photoproduct is observed at 3598 cm^{-1}. Because this band is sharp, it is clear that the intramolecular hydrogen bonding of CCC is broken by UV irradiation.

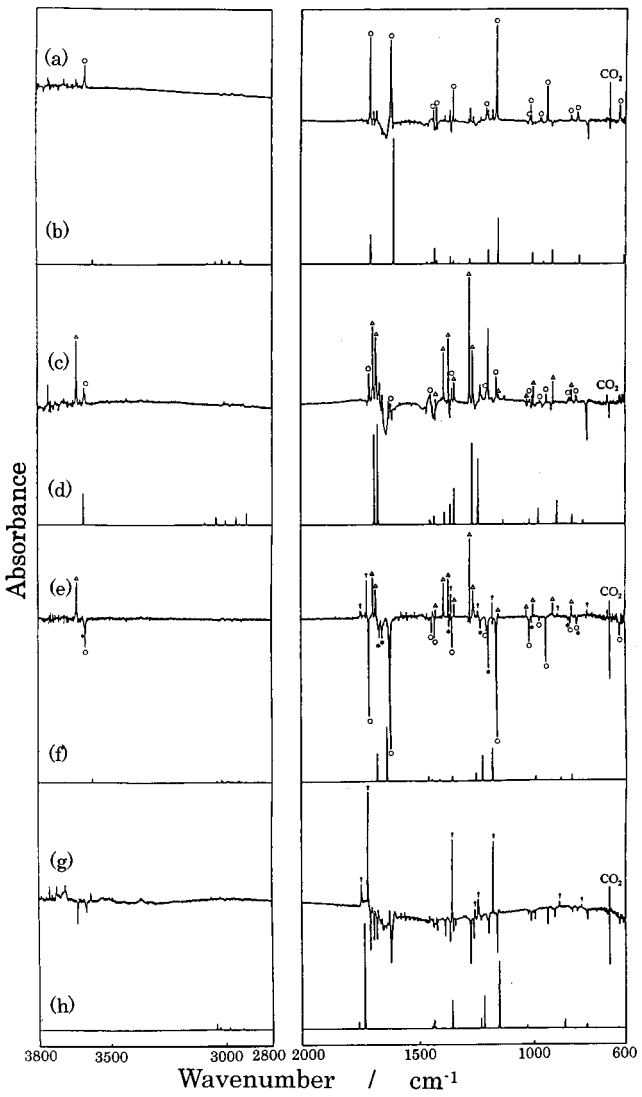

Figure 3. Comparison of observed matrix-isolation spectra with predicted spectral patterns calculated by DFT/B3LYP/6-31G*: (a) difference spectrum between those measured before and after 2-min UV irradiation; (b) calculated spectral pattern of CTC; (c) difference spectrum between those measured after 20- and 65-min UV irradiation; (d) calculated spectral pattern of TCT; (e) difference spectrum between those measured after 30-min UV irradiation through the UV-28 cut filter and following 10-min UV irradiation without the filter; (f) calculated spectral pattern of TTC; (g) difference spectrum between those measured after 250- and 370-min UV irradiation without the UV cut filter; (h) calculated spectral pattern of keto isomer. Bands marked with ○, △, and † are assigned to CTC, TCT, and keto isomer, respectively. Bands marked with ∗ denote an unknown species, tentatively assigned to TTC.

The strong C═O and C═C stretching bands are observed at 1704 and 1617 cm^{-1}, respectively. The difference in wavenumbers between these bands, 87 cm^{-1}, is close to that of the CCT or CTC isomer, as shown in Table 2. On the other hand, the strong band at 1159 cm^{-1} is consistent with the scaled wavenumber of the predicted strong band of CTC, 1151 cm^{-1}.

TABLE 4: Observed in Argon Matrixes and Calculated Wavenumbers (cm^{-1}) of UV-Induced Isomers of Acetylacetone

CTC		TCT		X		keto	
obsd[a]	calcd[b]	obsd[a]	calcd[b]	obsd[a]	calcd[b,c]	obsd[a]	calcd[b]
3598(m)	3565	3637(s)	3607	3602(m)	3572		3043
	3076		3087		3097		3043
	3041		3038		3037		3028
	3012		3036		3017		2986
	2983		2998		2992		2986
	2979		2956		2987		2966
	2933		2940		2941		2928
	2924		2910		2931		2928
1704(s)	1700	1688(s)	1683	1660(m)	1675	1740(w)	1754
1617(s)	1604	1677(s)	1668	1649(m)	1633	1714(s)	1728
	1464		1455		1461		1445
	1446		1448		1455		1440
	1439		1443		1441		1440
1438(w)	1431	1421(w)	1428		1438		1436
1425(w)	1422	1388(s)	1385		1408		1430
1352(m)	1362	1367(s)	1361		1366	1357(s)	1357
	1351	1342(m)	1344	1364(m)	1356		1357
	1278	1275(s)	1265		1256	1256(w)	1230
1203(w)	1194	1261(s)	1239	1228(m)	1227	1240(m)	1216
1159(s)	1151	1149(w)	1131	1194(s)	1184	1176(s)	1149
	1046		1037		1038		1108
1016(w)	1008	1025(w)	1015		1011		1044
1013(m)	1003		1003		993		1029
969(w)	957	995(m)	976	1001(w)	988		972
941(m)	919	912(m)	896	878(w)	881		910
838(w)	818	832(w)	829	811(w)	834	891(w)	867
811(w)	802		781		762	792(w)	769
625(m)	608		598		565		757

[a] Relative intensities are in parentheses. Symbols s, m, and w represent strong, medium, and weak, respectively. [b] A scaling factor of 0.96 is used. [c] Tentatively assigned to TTC.

Therefore, we assume that the product bands marked with ○ are assignable to CTC. The calculated spectral pattern of CTC, shown in Figure 3b, satisfactorily reproduces the observed spectrum in the whole region. The relative intensity of the 1617 cm^{-1} band seems to be smaller than that of the calculated value, because this band splits into two peaks. The observed and calculated wavenumbers of CTC are summarized in Table 4.

(3) TCT Isomer. The intensities of some peaks not assigned to CTC increased relatively upon subsequent UV irradiation. A difference spectrum between those spectra measured after 20-min and 65-min UV irradiation is shown in Figure 3c. The peaks marked with ○ in Figure 3a representing CTC are relatively weak in this irradiation period. Therefore, the peaks marked with a triangle (△) should be assigned to another photoproduct.

A new O−H stretching band is observed at the higher-wavenumber side of CTC, 3637 cm^{-1}. The C═O and C═C stretching bands are observed at 1688 and 1677 cm^{-1}. The difference, 11 cm^{-1}, is consistent with that of TCT or TTT. The strong bands, observed at 1275 and 1261 cm^{-1}, correspond to the scaled wavenumbers of the predicted bands of TCT, 1265 and 1239 cm^{-1}, instead of TTT, 1213 and 1180 cm^{-1}. Therefore, we assume that the peaks marked with △ are due to TCT. The calculated spectral pattern of TCT, shown in Figure 3d, satisfactorily reproduces the observed spectrum in the whole region, as summarized in Table 4.

There are bands still left unidentified in Figure 3c. The absorbance-growth behavior of the product bands is similar to that of TCT. To distinguish the product bands from TCT, another matrix sample was exposed to UV irradiation without the UV-28 cut filter for 10 min following the longer-wavelength irradiation for 30 min. The difference spectrum is shown in Figure 3e, where the intensities of a rapidly increasing product, CTC marked with ○, decreased. On the other hand, a slowly increasing product, TCT marked with △, increased in this period, while other bands of the other slowly increasing product, marked with ∗, decreased.

Because the vibrational wavenumber of the O−H stretching band, marked with ∗, is nearly equal to that of CTC, marked with ○, the ∗ bands may be assigned to TTC. However, the calculated spectral pattern of TTC shown in Figure 3f is slightly inconsistent with the observed spectrum. For example, the observed wavenumber difference between the C═O and C═C stretching bands, 15 cm^{-1}, is smaller than the calculated value, 43 cm^{-1}. One may thus assign the slowly increasing product to TTT because its calculated difference between the C═O and C═C stretching bands, 15 cm^{-1}, is consistent with the observed value. However, our calculation predicts that the O−H stretching band of TTT is nearly equal to that of TCT but not to that of CTC. Furthermore, the observed spectrum does not compare with any of the calculated spectral patterns of the other enol isomers or other possible species such as 1,3-pentadien-2,4-diol or 2-hydroxy-1-penten-4-one produced from acetylacetone by hydrogen atom migration. Hence, the assignment of this species remains unresolved at the present stage.

Because the CCC bands are not observed in Figure 3e, TCT must be produced from CTC or the unknown species, X, or both by shorter-wavelength ($\lambda < 280$ nm) UV irradiation. This finding implies that conformational change around the C═C bond occurs by the irradiation.

(4) Keto Isomer. In Figure 3e, there are increasing bands of a final product marked with †, except for the TCT bands. Figure 3g shows a difference spectrum of another sample between those spectra measured after 250- and 370-min UV irradiation without the UV cut filter. The intensities of the bands of CTC, TCT, and X decreased in this period, while those of the bands marked with † increased. There are weak and strong bands in the C═O stretching region. They can be assigned to the symmetric and antisymmetric C═O stretching modes of the keto isomer. The calculated spectral pattern of the keto isomer, which satisfactorily reproduces the observed spectrum of the final product, is shown in Figure 3h. The stronger C═O stretching band of the keto isomer, 1714 cm^{-1}, is slightly different from that in a deposited sample before UV irradiation, 1711 cm^{-1}, probably because of the site effect.

Additional photoreactions may be caused by UV irradiation with shorter wavelengths. We observed a strong band around 2100 cm^{-1}, which is assigned to ketene derivatives. Furthermore, a few bands are observed in the O−H stretching region. It is known by an analysis of the photofragment excitation spectrum that OH radical is produced from $\pi-\pi^*$ transition.[40,41] The vibrational wavenumber of OH radical is reported to be 3569 cm^{-1}.[42] A few bands appearing around 3600 cm^{-1} may be assigned to OH radical or its complexes with a coproduct.

Kinetics. Figure 4 shows the absorbance-growth behavior of infrared bands upon UV irradiation through the UV-28 cut filter, in which the 765, 1159, 1275, and 1194 cm^{-1} bands were chosen for CCC, CTC, TCT, and X, respectively. The reactant, CCC, decreased but did not vanish. This fact suggests that the photoreaction is in equilibrium or suggests the presence of the reactant species, which cannot take part in the reaction by site effects. The product CTC increases more rapidly than the products TCT and X. All the bands are almost unchanged after the 100-min UV irradiation.

When the first-order reactions are assumed, the absorbance of the product bands, A, are represented by the following

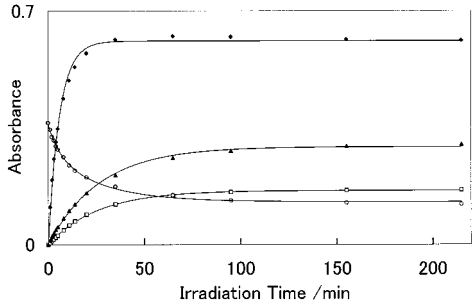

Figure 4. Absorbance-growth behavior of infrared bands. Symbols of ○, ◆, □, and ▲ represent the bands of 765 (CCC), 1159 (CTC), 1275 (TCT), and 1194 cm^{-1} (X), respectively. Solid lines represent the calculated values obtained by least-squares fittings; $A = A_\infty(1 - \exp(-kt))$ for the products and $A = A_1 \exp(-k_1 t) + A_2 \exp(-k_2 t) + A_3$ for the reactant, where k_1 and k_2 are 0.168 and 0.0383 min^{-1}, respectively.

equation using the corresponding rate constants k:

$$A = A_\infty(1 - \exp(-kt)) \quad (1)$$

where t and A_∞ represent irradiation time and absorbance at infinite time. Because the rate constants, k, clearly depend on the intensities of the absorbed radiation, we call them effective rate constants.

The effective rate constants obtained by least-squares fittings are 0.168 ± 0.018, 0.0391 ± 0.021, and 0.0376 ± 0.0030 min^{-1} for CTC, TCT, and X, respectively, where the uncertainties represent 3 times the standard deviations. The solid lines in Figure 4 represent the calculated values of the absorbance. It is understandable that the value for TCT is nearly equal to that for X, because their reactant is commonly CCC. However, it is strange that they are different from that for CTC. This discrepancy may be explained in terms of the site effect; the reaction path is determined by the condition of the argon-matrix site surrounding acetylacetone. In other words, there are at least two kinds of the reactant CCC supplies to produce CTC and TCT or X in the argon matrix. If this is true, the absorbance of CCC should be represented by

$$A = A_1 \exp(-k_1 t) + A_2 \exp(-k_2 t) + A_3 \quad (2)$$

where the first and second terms represent the absorbance of CCC forming to CTC and TCT (or X), respectively. The effective rate constant, k_1, was fixed to 0.168 min^{-1}, while k_2 was fixed to 0.0383 min^{-1}, an averaged value of those for TCT (0.0391 min^{-1}) and X (0.0376 min^{-1}). The third constant term is the absorbance of CCC that is unchanged upon UV irradiation. The three parameters, A_1, A_2, and A_3, are derived from the absorbance change of CCC to be 0.080 ± 0.024, 0.151 ± 0.018, and 0.128 ± 0.006 min^{-1}, respectively. This result means that 22% and 42% of CCC form to CTC and TCT (or X), respectively, while 36% of CCC is unchanged upon UV irradiation. Similar experiments of acetylacetone in xenon matrixes are in progress to explain the site effects.

Conclusion

Isomerization from cis to trans around the C−C, C═C, and C−O bonds of the CCC isomer in low-temperature argon matrixes was induced by UV irradiation through a UV-28 cut filter. The infrared bands of the photoproducts were assigned to CTC and TCT by a comparison with the spectral pattern calculated at the DFT/B3LYP/6-31G* level. Another product was tentatively assigned to TTC but could not be identified clearly. The effective rate constants for the products were derived from the absorbance-growth behavior of the infrared bands to be 0.168 ± 0.018, 0.0391 ± 0.021, and 0.0376 ± 0.0030 min^{-1} for CTC, TCT, and the unknown species, respectively. The discrepancy in the constants between CTC and TCT (or the unknown species) was explained in terms of the site effect. Hydrogen migration in the enol isomers produced by UV irradiation occurred to produce the keto isomer when the matrix sample was exposed to the UV radiation without the UV-28 cut filter. The observed spectrum of the keto isomer was consistent with the spectral pattern obtained by the DFT calculation.

Acknowledgment. The authors thank Professor Kozo Kuchitsu (Josai University) for his helpful discussion.

References and Notes

(1) Nakanishi, H.; Morita, H.; Nagakura, S. *Bull. Chem. Soc. Jpn.* **1977**, *50*, 2255.
(2) Lazaar, K. I.; Bauer, S. H. *J. Phys. Chem.* **1983**, *87*, 2411.
(3) Folkend, M. M.; Weiss-Lopez, B. E.; Chuvel, J. P.; True, N. S. *J. Phys. Chem.* **1985**, *89*, 3347.
(4) Schieringand, D. W.; Katon, J. E. *Appl. Spectrosc.* **1986**, *40*, 1049.
(5) Bauer, S. H.; Wilcox, C. F. *Chem. Phys. Lett.* **1997**, *279*, 122.
(6) Mecke, R.; Funck, E. *Z. Elektrochem.* **1956**, *60*, 1124.
(7) Ochterski, J. W.; Petersson, G. A.; Montgomery, J. A., Jr. *J. Chem. Phys.* **1996**, *104*, 2598.
(8) Ishida, T.; Hirata, F.; Kato, S. *J. Chem. Phys.* **1999**, *110*, 3938.
(9) Iijima, K.; Ohnogi, A.; Shibata, S. J. *J. Mol. Struct.* **1987**, *156*, 111.
(10) Egan, W.; Gunnarsson, G.; Bull, T. E.; Forsen, S. *J. Am. Chem. Soc.* **1977**, *99*, 4568.
(11) Cohen, B.; Weiss, S. *J. Phys. Chem.* **1984**, *88*, 3159.
(12) Shapet'ko, N. N.; Bazov, V. P. *Zh. Fiz. Khim.* **1989**, *63*, 2832.
(13) Gordon, M. S.; Koob, R. D. *J. Am. Chem. Soc.* **1973**, *95*, 5863.
(14) Dannenberg, J. J.; Rios, R. *J. Phys. Chem.* **1994**, *98*, 6714.
(15) Hinsen, K.; Roux, B. *J. Chem. Phys.* **1997**, *106*, 3567.
(16) Buemi, G.; Gandolfo, C. *J. Chem. Soc., Faraday Trans. 2* **1989**, *85*, 215.
(17) Marvi, J.; Grdadolnik, J. *J. Phys. Chem.* **2001**, *105*, 2039.
(18) Marvi, J.; Grdadolnik, J. *J. Phys. Chem.* **2001**, *105*, 2045.
(19) Vereiov, D.; Bercovici, T.; Fisher, E.; Masur, Y.; Vogev, A. *J. Am. Chem. Soc.* **1973**, *95*, 8173.
(20) Roubin, P.; Chiavassa, T.; Verlaque, P.; Pizzala, L.; Bodot, H. *Chem. Phys. Lett.* **1990**, *175*, 655.
(21) Chiavassa, T.; Verlaque, P.; Pizzala, L.; Roubin, P. *Spectrochim. Acta* **1994**, *50A*, 343.
(22) Labanowski, J., Andzelm, J. W., Eds. *Density Functional Methods in Chemistry*; Springer-Verlag: New York, 1991.
(23) Seminario, J. M., Politzer, P., Eds. *Modern Density Functional Theory: A Tool for Chemistry*; Elsevier: Amsterdam, 1995.
(24) Kudoh, S.; Takayanagi, M.; Nakata, M. *Chem. Phys. Lett.* **2000**, *322*, 363.
(25) Kudoh, S.; Takayanagi, M.; Nakata, M. *J. Photochem. Photobiol., A* **1999**, *123*, 25.
(26) Kudoh, S.; Takayanagi, M.; Nakata, M. *Chem. Phys. Lett.* **1999**, *308*, 403.
(27) Kudoh, S.; Takayanagi, M.; Nakata, M. *J. Mol. Struct.* **1999**, *475*, 253.
(28) Kudoh, S.; Onoda, K.; Takayanagi, M.; Nakata, M. *J. Mol. Struct.* **2000**, *524*, 61.
(29) Kudoh, S.; Takayanagi, M.; Nakata, M. *J. Mol. Struct.* **1997**, *413/414*, 365.
(30) Kudoh, S.; Takayanagi, M.; Nakata, M.; Ishibashi, T.; Tasumi, M. *J. Mol. Struct.* **1999**, *479*, 41.
(31) Kudoh, S.; Takayanagi, M.; Nakata, M.; Tanaka, N.; Shibuya, K. *J. Mol. Struct.* **2000**, *524*, 251.
(32) Kudoh, S.; Uechi, T.; Takayanagi, M.; Nakata, M.; Frei, H. *Chem. Phys. Lett.* **2000**, *328*, 283.
(33) Frisch, M. J.; Trucks, G. W.; Schlegel, H. B.; Scuseria, G. E.; Robb, M. A.; Cheeseman, J. R.; Zakrzewski, V. G.; Montgomery, J. A., Jr.; Stratmann, R. E.; Burant, J. C.; Dapprich, S.; Millam, J. M.; Daniels, A. D.; Kudin, K. N.; Strain, M. C.; Farkas, O.; Tomasi, J.; Barone, V.; Cossi, M.; Cammi, R.; Mennucci, B.; Pomelli, C.; Adamo, C.; Clifford, S.; Ochterski, J.; Petersson, G. A.; Ayala, P. Y.; Cui, Q.; Morokuma, K.; Malick, D. K.; Rabuck, A. D.; Raghavachari, K.; Foresman, J. B.; Cioslowski, J.; Ortiz, J. V.; Stefanov, B. B.; Liu, G.; Liashenko, A.; Piskorz, P.; Komaromi, I.; Gomperts, R.; Martin, R. L.; Fox, D. J.; Keith, T.; Al-Laham, M. A.;

Peng, C. Y.; Nanayakkara, A.; Gonzalez, C.; Challacombe, M.; Gill, P. M. W.; Johnson, B. G.; Chen, W.; Wong, M. W.; Andres, J. L.; Head-Gordon, M.; Replogle, E. S.; Pople, J. A. *Gaussian 98*, revision A.6; Gaussian, Inc.: Pittsburgh, PA, 1998.

(34) Becke, A. D. *J. Chem. Phys.* **1993**, *98*, 5648.

(35) Lee, C.; Yang, W.; Parr, R. G. *Phys. Rev.* **1988**, *37B*, 785.

(36) Chiavassa, T.; Roubin, P.; Pizzala, L.; Verlaque, P.; Allouche, A.; Marinelli, F. *J. Phys. Chem.* **1992**, *96*, 10659.

(37) Chiavassa, T.; Verlaque, P.; Pizzala, L.; Allouche, A.; Roubin, P. *J. Phys. Chem.* **1993**, *97*, 5917.

(38) Wong, M. W. *Chem. Phys. Lett.* **1996**, *256*, 391.

(39) Scott, A. P.; Radom, L. *J. Phys. Chem.* **1996**, *100*, 16502.

(40) Yoon, M.-C.; Choi, Y. S.; Kim, S. K. *Chem. Phys. Lett.* **1999**, *300*, 207.

(41) Yoon, M.-C.; Choi, Y. S.; Kim, S. K. *J. Chem. Phys.* **1999**, *110*, 11850.

(42) Herzberg, G. *Spectra of Diatomic Molecules*; Molecular Spectra and Molecular Structure, 2nd ed., Vol. 1; Robert E. Krieger Publishing Co.: Malabar, Florida, 1989.